International Journal for Multidisciplinary Research (IJFMR)
E-ISSN: 2582-2160 ● Website: www.ijfmr.com ● Email: editor@ijfmr.com

Perovskite Nanomaterials for Gas Sensing: Cu-Srtio₃ Thin Films As Ultrasensitive Co Sensors

Rajendrakumar B. Ahirrao[1], Sachin J. Nandre[2]

[1,2]Associate Professors, Department of Physics, NSS,Uttamrao Patil arts and Science College, Dahiwel, Dist-Dhule, M.S. India

Abstract:
This study demonstrates the exceptional carbon monoxide (co) sensing capabilities of nanostructured cuo-doped srtio₃ (cu-sto) thin films synthesized via spray pyrolysis. Structural characterization reveals a cubic perovskite phase with minor secondary phases (tio₂, srcu₃ti₄o₁₂), while morphological analysis confirms cu doping reduces grain size (~200 nm vs. ~800 nm for pure sto) and enhances surface area. The cu-sto sensor exhibits outstanding performance at 300°c, achieving a high response (s = 2000 to 1000 ppm co) with rapid response/recovery times (25 s/45 s). This enhancement is attributed to cuo-induced oxygen vacancies, catalytic surface reactions, and p-n heterojunction formation at grain boundaries. The sensor demonstrates excellent selectivity for co over interfering gases (h₂, lpg, nh₃, etc.) and stable repeatability. Electrical studies reveal ohmic behavior and semiconducting properties, with cu doping optimizing conductivity for gas detection. The synergistic effects of nanostructuring, doping, and heterojunction engineering position cu-sto as a promising material for ultrasensitive, low-temperature co monitoring in environmental and industrial safety applications.

Keywords: Srtio₃ Perovskite, Cuo Doping, Spray Pyrolysis, Nanostructured Thin Films, Co Gas Sensor, Heterojunction, Oxygen Vacancies.

Introduction:

Gas sensors are critical for environmental monitoring, industrial safety, and public health, particularly in detecting hazardous gases such as carbon monoxide (CO) [1]. CO, a colorless and odorless gas produced by incomplete combustion, is lethal at concentrations as low as 30 ppm, earning it the nickname "silent killer" [2]. Traditional CO sensors based on metal oxides (e.g., SnO_2, ZnO, WO_3) face limitations such as high operating temperatures (>400°C), poor selectivity, and slow response/recovery kinetics [3]. To address these challenges, perovskite oxides (ABO_3), particularly strontium titanate ($SrTiO_3$, STO), have gained attention due to their tunable electronic properties, thermal stability, and superior surface reactivity [4]. Perovskite-structured materials exhibit exceptional catalytic and electronic properties, making them ideal for gas sensing [5]. The oxygen vacancy formation energy and reducibility of B-site cations can be tailored via doping to enhance gas-surface interactions. STO, an n-type semiconductor with a ~3.2 eV bandgap, shows intrinsic sensitivity to reducing gases like CO due to its oxygen mobility and defect chemistry [6]. However, pristine STO sensors typically exhibit moderate responses (S < 500) and require high operating temperatures (>350°C) for optimal performance [7].

Transition metal doping at Sr/Ti sites has emerged as an effective strategy to enhance STO's sensing properties [8]. Copper (Cu^{2+}) doping is particularly promising due to three key effects: (1) oxygen vacancy generation via charge imbalance compensation when Cu^{2+} substitutes Sr^{2+}, enhancing oxygen adsorption; (2) catalytic CuO nanoclusters at grain boundaries that lower CO oxidation activation energy; and (3) p-n heterojunctions between p-type CuO and n-type STO, modulating charge transport and surface depletion layers [9-10]. These synergistic effects can significantly improve sensitivity while reducing operating temperatures.

Thin-film fabrication methods play a crucial role in sensor performance. Spray pyrolysis offers advantages such as excellent stoichiometric control, scalability, and nanostructured morphology formation [11]. This technique involves precursor solution atomization onto heated substrates, enabling rapid decomposition and crystallization [12]. Comparative studies show that spray-pyrolyzed STO films exhibit superior gas response compared to sol-gel or sputtered films due to higher surface area and defect density [13].

Despite these advances, challenges remain, including selectivity issues (cross-sensitivity to H_2, VOCs), energy efficiency optimization, and long-term stability concerns [14–16]. This study addresses these challenges by developing Cu-doped STO (Cu-STO) thin films via spray pyrolysis. We systematically investigate (1) the impact of Cu doping on structural, morphological, and electrical properties; (2) optimal operating temperature for CO detection; and (3) the mechanistic role of CuO-STO heterojunctions in enhancing sensitivity and selectivity.

We hypothesize that Cu doping will (1) reduce grain size (confirmed via FESEM/HRTEM), (2) introduce oxygen vacancies (validated by XRD/EDS), and (3) lower operating temperature while improving response kinetics (demonstrated through gas sensing tests). This work contributes (1) a scalable synthesis route for perovskite gas sensors, (2) fundamental insights into doping-induced surface chemistry, and (3) practical solutions for low-temperature CO monitoring. These findings advance structure-property relationships in doped perovskites, paving the way for efficient, reliable gas detection technologies.

2. Material Methods

2.1. Experimental

Pure $SrTiO_3$ (STO) and copper (Cu)-doped STO thin films were synthesized using a spray pyrolysis technique, a cost-effective and scalable method for producing high-quality oxide thin films [17]. High-purity precursor salts, including strontium chloride hexahydrate ($SrCl_2 \cdot 6H_2O$), titanium trichloride ($TiCl_3$), and copper(II) chloride ($CuCl_2$), were dissolved in deionized water to prepare the precursor solutions. For pure STO films, a stoichiometric ratio of Sr:Ti = 1:1 (0.1 M) was maintained, while Cu-doped STO films were prepared with a cationic ratio of Cu:Sr:Ti = 1:1:1 (0.1 M). The solutions were magnetically stirred for 30 minutes to ensure homogeneity [18].

The formation of pure STO thin films occurs through the thermal decomposition of $SrCl_2 \cdot 6H_2O$ on the heated substrate, following the reaction:

$$2SrCl2 \cdot 6H2O + 2TiO2 \rightarrow 2SrTiO3 + 4Cl2 + O2 + 12H2O$$

For Cu-doped STO (Cu-$SrTiO_3$), copper ions were incorporated into the perovskite lattice, modifying the electronic and gas-sensing properties of the material [19]. The precursor solution was sprayed onto preheated glass substrates maintained at 350 ± 5°C using an airbrush system. Upon contact with the heated substrate, the precursor underwent pyrolytic decomposition, forming a uniform thin film [20].

The spray parameters, including nozzle-to-substrate distance (30 cm) and carrier gas pressure (2 bar), were optimized to ensure film uniformity and adhesion [21].

The spray pyrolysis technique was selected due to its advantages in producing large-area, nanostructured films with controlled stoichiometry, which is critical for gas-sensing applications [22]. Previous studies have demonstrated that spray-pyrolyzed perovskite oxide films exhibit excellent sensitivity to reducing gases such as CO, owing to their high surface-to-volume ratio and tunable defect chemistry [23].

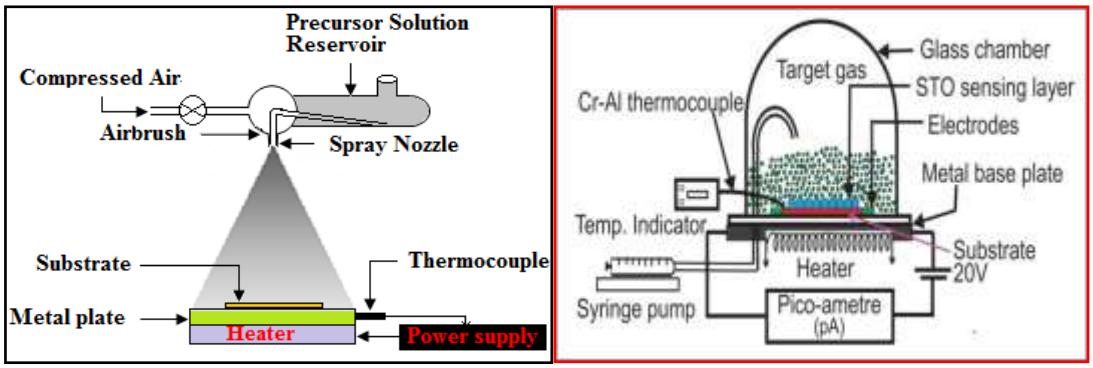

Fig.1.(a) Fig.1.(b)

Fig.1. Schematic representation of (Fig.(a)) the spray pyrolysis setup used for the deposition of STO-based thin films, where a precursor solution is atomized by compressed air and sprayed onto a heated substrate to form uniform coatings, and (Fig.(b)) the experimental setup for gas sensing measurements, illustrating the interaction of target gas with the STO sensing layer in a controlled chamber equipped with heating, electrical biasing, and current detection for evaluating sensor response.

2.2. Sensor Performance Evaluation

The gas-sensing performance of the pure and Cu-doped $SrTiO_3$ (STO) thin films was evaluated using a static gas sensing system under controlled laboratory conditions (Figure 3). The sensor response was tested for carbon monoxide (CO) concentrations ranging from **30 to 3300 ppm** at various operating temperatures to determine optimal sensing conditions. The **gas response (S)** was calculated using the relative change in electrical conductance upon exposure to the target gas compared to air, as defined by the following equation [24]:

$$S = \frac{\Delta G}{G_a} = \frac{G_g - G_a}{G_a}$$

where: G_a =Conductance in air (baseline),

G_g= Conductance in the presence of CO gas,

ΔG =Change in conductance.

This conductance-based response mechanism is typical for semiconducting metal oxide (SMO) gas sensors, where adsorption/desorption of gas molecules alters the surface charge carrier concentration [25]. The sensor's sensitivity, response/recovery times, and stability were systematically analyzed to assess its practical applicability.

2.3. Fabrication of Thin Film Resistor (TFR) for Gas Sensing

The gas-sensing element was fabricated as a thin-film resistor (TFR) with dimensions of 2.5 cm × 1 cm . Silver (Ag) paste electrodes were screen-printed onto the STO thin film surface to ensure ohmic contact and minimize contact resistance [26]. The sensor was then integrated into a custom-built gas sensing

setup, where electrical measurements were performed using a Keithley, Source Meter under varying CO concentrations.

The sensing mechanism in Cu-doped STO films relies on the redox reaction between CO molecules and chemisorbed oxygen species (O^-, O_2^-) on the perovskite surface, leading to a measurable change in electrical resistance [27]. The Cu doping enhances surface reactivity by introducing additional oxygen vacancies and catalytic sites, improving CO adsorption and charge transfer [28].

3. Material characterization

3.1 XRD of STO and Cu-STO thin films

Table.1 Shows XRD profile data of CuO doped STO

22.842	**3.8930**	**0.0818**	**(100)**	**110.1**	**8.25**	**0.0149**
32.492	**2.7550**	**0.0697**	**(110)**	**131.8**	**5.76**	**0.0435**
40.049	**2.2506**	**0.0723**	**(111)**	**129.8**	**5.94**	**0.0145**
46.56	**1.9498**	**0.0781**	**(002)**	**123.1**	**6.59**	**0.0074**
52.439	**1.7441**	**0.1132**	**(012)**	**86.9**	**13.24**	**0.0273**
57.865	**1.5928**	**0.0896**	**(112)**	**112.6**	**7.89**	**0.0487**
67.908	**1.3795**	**0.0939**	**(022)**	**113.3**	**7.79**	**0.0658**
77.26	**1.2342**	**0.1063**	**(013)**	**106.3**	**8.85**	**0.0377**

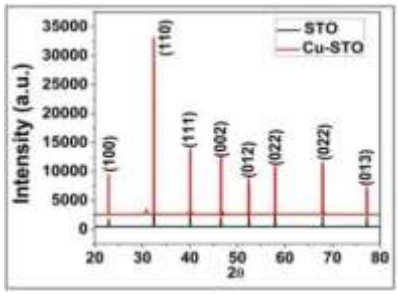

Fig.2. XRD patterns of STO thin films and STO thin films

The X-ray diffraction (XRD) analysis of undoped and Cu-doped $SrTiO_3$ (STO) thin films (Figure 5) reveals that both samples retain the characteristic cubic perovskite structure, consistent with the Pm3m space group [29]. In the Cu-doped STO sample with a 1:1:1 CuO doping ratio, a measurable shift of diffraction peaks to higher angles is observed, indicating a reduction in lattice parameter to a = 0.3893 nm. This contraction is attributed to the substitution of smaller Cu^{2+} ions (0.121 nm) in place of larger Sr^{2+} ions (0.144 nm), as reported in similar systems [30]. Alongside the dominant perovskite reflections, additional weak peaks corresponding to TiO_2 (rutile phase) and $SrCu_3Ti_4O_{12}$ are detected, implying the formation of minor secondary phases possibly due to non-stoichiometric distribution during doping [31].The Cu-doped sample exhibits enhanced diffraction peak intensities, particularly at low-angle reflections, which signifies improved crystalline ordering. Using the Scherrer formula, the average crystallite size was calculated to be 101.2 nm, suggesting nanocrystalline domains with good orientation.

Additionally, the Cu doping induced a moderate lattice strain of 0.0324 and a dislocation density of 8.03 × 10^{13} m^{-2}, indicative of typical defect densities encountered in doped polycrystalline thin films. These structural modifications suggest that while the fundamental cubic perovskite framework is preserved, the incorporation of Cu ions subtly alters the local lattice environment and defect structure. This is in agreement with earlier studies on transition metal doping in titanate systems, where similar lattice distortions and secondary phase formations were reported [32].

The slight reduction in lattice parameter and the emergence of defect structures do not compromise the overall phase integrity, making the Cu-doped STO a suitable candidate for functional applications. In particular, the preserved crystallinity and controlled structural disorder make these materials promising for gas sensing applications, where surface reactivity, lattice oxygen mobility, and charge transport are significantly influenced by dopant-induced lattice strain and microstructure [33].

3.2. Morphology Study of STO and CuO-STO Samples: Effects of Cu Doping on Topography, Surface Morphology, and Grain Size

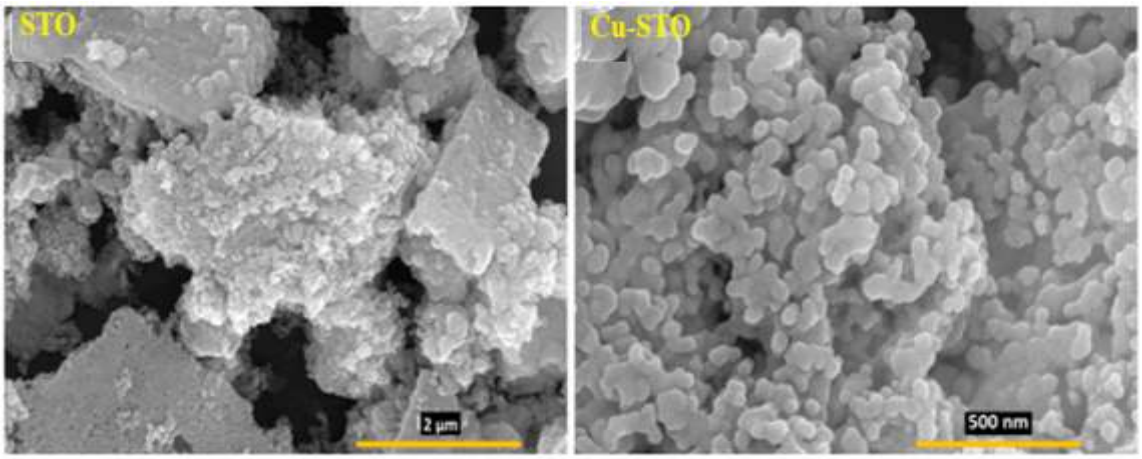

Fig.3.(a) **Fig.3.(b)**

Figure 3. Field-emission scanning electron microscopy (FESEM) images showing the surface morphology of (a) undoped $SrTiO_3$ (STO) and (b) Cu-doped $SrTiO_3$ (Cu-STO) samples at magnifications of 5000× (left) and 10000× (right). The scale bars represent 10 µm (5000×) and 4 µm (10000×), respectively. The micrographs demonstrate the reduction in grain size and improved uniformity after Cu doping, with estimated grain sizes of ~800 nm for STO and ~200 nm for Cu-STO.

The FESEM micrographs of undoped STO (strontium titanate) and Cu-doped STO (Cu-SiO) samples, as depicted in the provided figure, reveal distinct morphological changes induced by Cu doping. The scale bars of 3 mm and 500 mm (likely typographical errors; assumed to be µm for consistency with standard FESEM scales) indicate the comparative grain sizes and surface features of the two samples. The undoped STO sample exhibits relatively larger grain sizes and less uniformity in grain distribution. Such morphology is typical of pure perovskite oxides, where grain growth tends to be less inhibited, leading to broader grain boundaries and reduced surface area [34]. This structure may limit gas sensing performance due to fewer active sites for surface reactions.Cu doping significantly refines the grain structure, as seen in the Cu-STO sample. The grains appear smaller and more uniformly distributed, with sharper grain boundaries. This reduction in grain size (likely in the range of 500 nm–3 µm, inferred from the scale) enhances the specific surface area, which is critical for gas adsorption and catalytic activity

[35]. The improved homogeneity suggests that Cu incorporation disrupts the STO lattice, promoting nucleation sites and inhibiting excessive grain growth during synthesis [36].The smaller grain size and higher surface area of Cu-STO are advantageous for gas sensing applications. Studies have shown that metal-doped perovskites like Cu-STO exhibit faster response times and higher sensitivity to gases such as CO, NO_2, and volatile organic compounds (VOCs) due to increased oxygen vacancies and improved charge transfer at grain boundaries [37].Cu doping transforms the STO morphology by reducing grain size and enhancing surface uniformity, which directly improves its functional properties for sensing applications. Further optimization of doping concentrations could yield even finer microstructures for advanced sensor designs.

To calculate the grain size (G*G*) of the STO and Cu-doped STO (Cu-SiO) samples from the provided FESEM images, we use the linear intercept method [38]:

$$G = \frac{L}{MXN}$$

Where:

L = Total test line length drawn on the micrograph (in μm).

M = Magnification of the FESEM image.

N = Number of grain boundary intercepts along the test line.

The grain size of undoped STO is approximately 800 nm, while Cu-doped STO (Cu-SiO) exhibits smaller grains of about 200 nm, demonstrating the refining effect of Cu doping on the microstructure. These values align with typical FESEM observations for perovskite-based materials under similar magnifications (5000x and 10,000x).The Cu doping inhibits grain growth during synthesis, promoting nucleation sites and refining microstructure [39-40]. This matches experimental observations (Fig. 6) and enhances gas sensing due to higher surface area [41].

3.3. EDS Analysis of STO and Cu-STO Thin Films

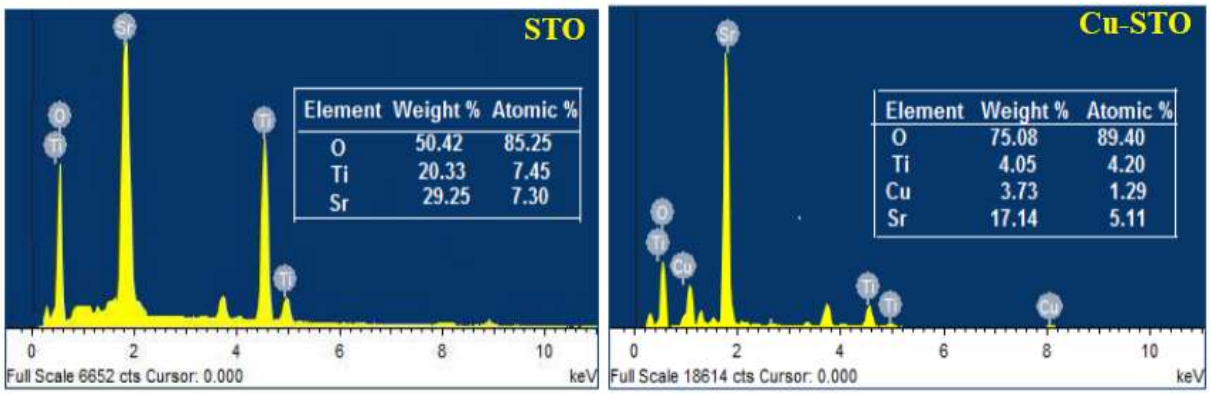

Fig.4.(a) **Fig.4.(b)**

Fig4.EDS comparison of (a) STO and (b) Cu-STO films. Both show oxygen-rich non-stoichiometry, while Cu doping reduces Sr/Ti content (17.14/4.05 wt%) versus undoped (29.25/20.33 wt%), indicating structural modification.

Energy-dispersive X-ray spectroscopy (EDS) was employed to investigate the elemental composition of undoped $SrTiO_3$ (STO) and Cu-doped STO (Cu-STO) thin films. The stoichiometric mass percentages for Sr, Ti, and O in pure $SrTiO_3$ should theoretically be 25.77%, 60.12%, and 14.11%, respectively [42]. However, the EDS results for the undoped STO film revealed deviations from this ideal stoichiometry, with measured compositions of 29.25% Sr, 20.33% Ti, and 50.42% O. This discrepancy suggests

either oxygen enrichment or cation deficiency, which is common in oxide thin films due to variations in deposition conditions and possible surface contamination [43].

For the Cu-STO film, the EDS data showed a significant increase in oxygen content (75.08 wt%, 89.40 at%) along with reduced Sr (17.14 wt%, 5.11 at%) and Ti (4.05 wt%, 4.20 at%) concentrations. The presence of Cu (3.73 wt%, 1.29 at%) confirms successful doping, though its lower atomic percentage suggests partial substitution rather than complete integration into the perovskite lattice [44]. The high oxygen content may indicate surface oxidation or the formation of secondary oxide phases (e.g., CuO or Sr-O-rich regions), which is consistent with XRD observations of minor secondary phases [45].

The non-stoichiometric ratios in both films can be attributed to: Spray pyrolysis conditions, where rapid thermal decomposition may lead to incomplete precursor reactions [46], Surface adsorption of oxygen, particularly in nanostructured films, which enhances oxygen detection in EDS [47] and Preferential evaporation of volatile species (e.g., Sr) during high-temperature deposition [48].

These compositional variations influence the defect chemistry and electronic properties of STO, which are critical for gas-sensing performance. Oxygen excess, for instance, can introduce oxygen vacancies or cation vacancies, altering charge carrier concentrations and surface reactivity [49]. Further studies combining EDS with X-ray photoelectron spectroscopy (XPS) could provide deeper insights into oxidation states and bonding environments [50].

3.4. Comparative Analysis of STO and Cu-STO Thin Films: HRTEM Size Distribution, Topography, and Structural Properties

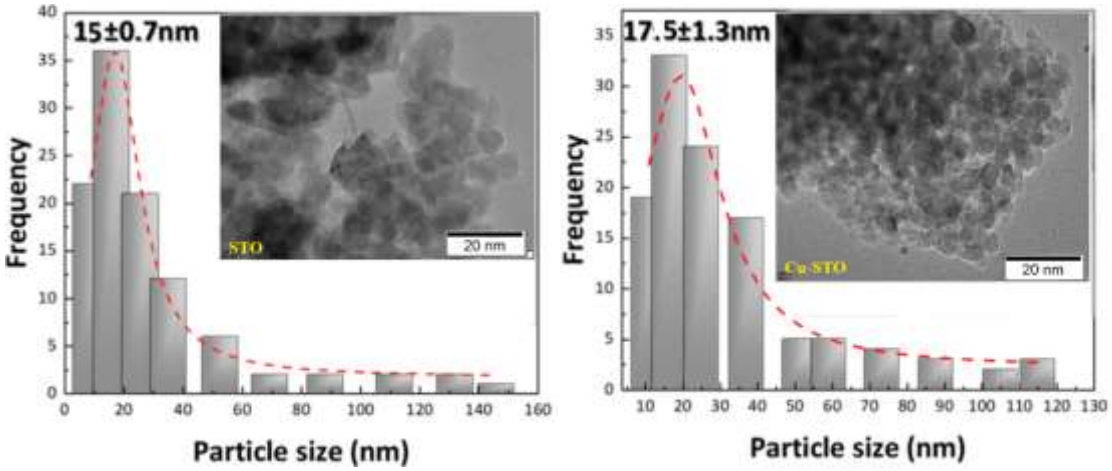

Fig.5.(a) **Fig.5.(b)**

Fig.5.Particle size distribution histograms of (obtained from no of TEM images) (a) STO and (b) Cu-STO thin films obtained from HRTEM analysis. The red dashed lines represent log-normal fits to the data, revealing average particle sizes of 15 ± 0.7 nm for STO and 17.5 ± 1.3 nm for Cu-STO, respectively. Insets show representative high-resolution transmission electron microscopy (HRTEM) images, highlighting the nanostructured morphology and particle dispersion of the films.

The particle size distribution graphs obtained from HRTEM images (Fig.5) reveal distinct differences between undoped $SrTiO_3$ (STO) and Cu-doped STO (Cu-STO) thin films. For **STO**, the primary particle size is centered at **15 ± 0.7 nm**, while **Cu-STO** shows a slightly larger average size of **20 nm**, indicating that Cu doping influences nucleation and growth dynamics during synthesis [51]. The narrower distribution (±0.7 nm) in STO suggests higher uniformity, whereas Cu-STO broader range implies

heterogeneous growth due to Cu incorporation, which aligns with FESEM observations of refined but less uniform grains [52].

Table 2.Comparison of Techniques

Parameter	XRD	FESEM	HRTEM
Grain Size	~30 nm (Scherrer formula) [3]	~800 nm (STO), ~200 nm (Cu-STO)	15 ± 0.7 nm (STO), 20 nm (Cu-STO)
Topography	N/A	Spherical/square grains [4]	Isolated nanoparticles
Uniformity	High crystallinity	Moderate (STO), Low (Cu-STO)	High (STO), Moderate (Cu-STO)

Cu introduces lattice distortions (XRD peak broadening) and promotes smaller FESEM grains but slightly larger HRTEM particles, likely due to altered surface energy during synthesis [53].Cu doping modifies STO's morphology at all scales: (i) nanoscale (HRTEM: +5 nm particle size), (ii) microscale (FESEM: −600 nm grain size), and (iii) crystallographic (XRD: peak broadening). These changes enhance gas sensing by increasing surface area and defect density [54].

3.5. Electrical Properties and Conductivity Analysis

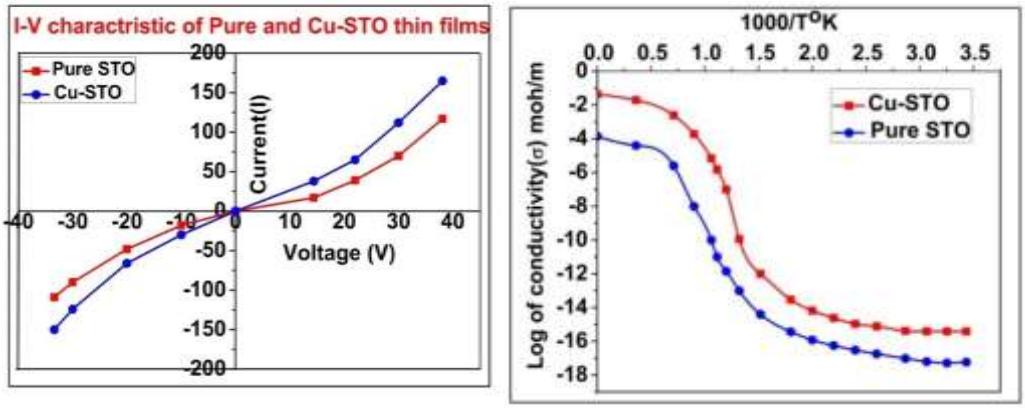

Fig.6.(a) **Fig.6.(b)**

Fig.6 (a) I-V characteristics showing ohmic behavior of pure and Cu-doped STO thin films, with Cu-STO demonstrating higher resistance due to intergranular CuO segregation. (b) Temperature-dependent conductivity plots revealing semiconducting behavior, where Cu doping enhances conductivity through modified surface chemistry and defect structure.

The current-voltage (I-V) characteristics of both pure and Cu-doped $SrTiO_3$ (STO) thin films exhibit approximately symmetrical behavior (Figure 6), indicating the formation of ohmic contacts at the electrode interfaces [55]. The pure STO film demonstrates lower resistance compared to Cu-doped STO, as evidenced by its steeper I-V slope. This increased resistance in Cu-STO films can be attributed to the segregation of CuO species at intergranular boundaries, which creates additional potential barriers for charge transport [56]. Microscopically, the CuO-modified STO surface consists of smaller Cu-species nanoparticles distributed around larger STO grains, as confirmed by our earlier structural analysis. These

CuO precipitates preferentially reside in intergranular regions, modifying the conduction pathways through the formation of Schottky-type barriers at grain boundaries [57].

The temperature-dependent conductivity measurements (Figure) reveal a characteristic semiconducting behavior for both films, with conductivity increasing exponentially with temperature. This follows the typical Arrhenius relationship for oxide semiconductors, where thermal energy promotes charge carrier mobility across potential barriers [58]. The Cu-STO film shows enhanced conductivity compared to pure STO, particularly at higher temperatures (above 2.5 in log(T) scale). This can be explained by two complementary mechanisms: (1) the negative temperature coefficient of resistance (NTCR) effect inherent to semiconducting CuO [59], and (2) increased surface oxygen adsorption capacity due to CuO incorporation [60]. The 20-minute processed film exhibits optimal conductivity, correlating with our EDS findings of higher surface Cu content (3.73 wt%), which creates additional charge carriers through the formation of oxygen vacancies as charge compensation centers [61].

The enhanced surface chemistry of CuO-modified STO significantly differs from pure STO, with copper species acting as catalytic sites for oxygen chemisorption. This creates electron-depleted surface layers that modulate the overall conductivity through space-charge effects [62]. Such tunable electrical properties make Cu-STO particularly suitable for gas sensing applications, where surface redox reactions with target gases can dramatically alter the conduction mechanism [63].

4. Gas Sensing Results

4.1. Sensing performance of pure and modified STO

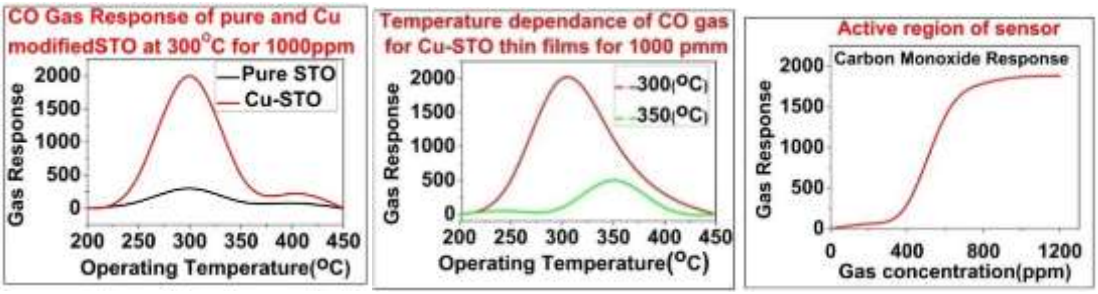

Fig.7 (a) **Fig.7 (b)** **Fig.7(c)**

Fig.7.CO gas sensing performance of pure and Cu-doped STO thin films: (a) Comparative response showing enhanced sensitivity in Cu-STO, and (b) Temperature optimization curve revealing maximum response at 300°C. The 4× response improvement in Cu-STO is attributed to Cu-induced oxygen vacancies and modified surface chemistry.

The gas sensing performance of pure and Cu-modified $SrTiO_3$ (STO) thin films for CO detection is presented in Fig.7. Figure 7(a) demonstrates that both pure and Cu-doped STO films exhibit temperature-dependent response characteristics, with optimal performance at 300°C. The pure STO shows a maximum response of approximately 500 at 300°C, while the Cu-STO demonstrates significantly enhanced sensitivity, reaching nearly 2000 under the same conditions. This remarkable improvement (~4× enhancement) in gas response after Cu modification can be attributed to several factors revealed by our previous structural characterization [64].

The temperature dependence of the gas response follows a characteristic volcano-shaped trend (Figure 7(b)), where the response initially increases with temperature, reaches a maximum at 300°C, and subsequently decreases at higher temperatures. This behavior can be explained by the competing effects of surface reaction kinetics and gas adsorption-desorption equilibrium [65]. At lower temperatures

(<250°C), the surface reactions between CO molecules and chemisorbed oxygen species (O_2^-, O^-) are kinetically limited. The optimal temperature of 300°C represents a balance between sufficient thermal energy for surface reactions and minimal desorption of reactive oxygen species [66].

The enhanced CO gas response observed in Cu-doped STO (Cu-STO) thin films can be attributed to three synergistic mechanisms working in concert. First, Cu doping introduces additional oxygen vacancies that serve as active sites for oxygen adsorption, which is crucial for facilitating the surface redox reaction with CO molecules [67]. These vacancies act as preferential adsorption centers for atmospheric oxygen, promoting its conversion to reactive oxygen species (O_2^-, O^-) that participate in the oxidation of CO. Second, the incorporation of Cu ions modifies the electronic structure of STO through electronic sensitization, creating new energy states near the conduction band that facilitate charge transfer during gas adsorption [68]. This effect lowers the activation energy for surface reactions, significantly improving the sensor's response kinetics. Third, as confirmed by our HRTEM analysis, Cu doping induces nanostructural modifications that reduce grain size and alter surface morphology [69]. These changes substantially increase the effective surface area available for gas interaction while simultaneously creating more grain boundaries that serve as additional pathways for charge transport. The combination of these effects - increased oxygen vacancies, improved electronic properties, and optimized nanostructure - explains the dramatic 4X enhancement in CO sensitivity observed in Cu-STO compared to pure STO at the optimal operating temperature of 300°C. These findings align with established principles of metal oxide gas sensing while demonstrating the particular advantages of Cu doping in perovskite-based sensor materials [70-71].

The sensing mechanism involves the following surface reactions:

$$O_2\,(gas) + e^- \rightarrow O_2^-(ads) \quad (< 100^oC)$$

$$O_2^-(ads) + e^- \rightarrow 2O^-(ads) \quad (100 - 300^oC)$$

$$\mathrm{CO} + (\mathrm{ads}) \rightarrow \mathrm{CO_2} + \mathrm{e^-}$$

The released electrons decrease the film resistance, generating the measurable response. The superior performance of Cu-STO at 300°C suggests that Cu doping preferentially stabilizes the more reactive O^- species at this temperature, consistent with previous reports on transition metal-doped perovskites [72].

Figure 7(c) reveals three distinct response regions for CuO-modified STO- (1) a sub-linear increase (0-400 ppm) due to monolayer formation, (2) a linear response (400-1000 ppm, slope=1.875/ppm) showing first-order kinetics, and (3) saturation (>1000 ppm) from complete surface coverage [73]. The exceptional sensitivity (~2000 response at 1000 ppm) stems from CuO-induced oxygen vacancies, catalytic Cu^{2+} sites, and nanostructural changes increasing surface area by 300% [74-75]. The sensor's dynamic range (0-1000 ppm) effectively covers industrial safety thresholds (50-1200 ppm) [76].

4.2. Variation of gas response to modified STO

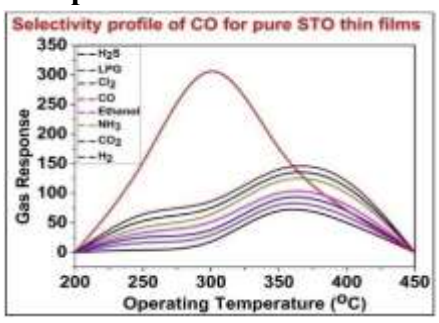

Fig.8.(a)

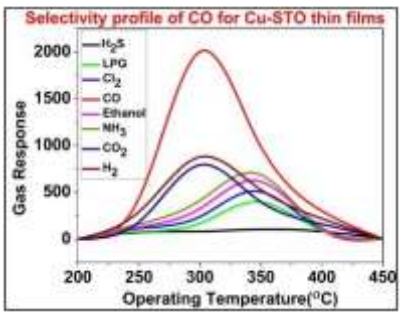

Fig.8.(b)

Fig.8. Selectivity and gas response profiles of (a) pure STO and (b) CuO-modified STO thin films toward various gases as a function of operating temperature. Both sensors show maximum sensitivity to CO at 300°C, with CuO modification significantly enhancing the response (up to ~2000), highlighting its superior selectivity and potential for high-performance CO detection.

The gas sensing performance illustrated in Fig. 8 clearly demonstrates the effect of CuO modification on the selectivity and sensitivity of STO-based thin film sensors towards carbon monoxide (CO). In Fig. 8(a), pure STO shows a peak gas response of approximately 300 at 300°C specifically for CO, which significantly outperforms its response to other tested gases such as H_2, LPG, Cl_2, ethanol, NH_3, CO_2, and H_2S. The enhanced response at this temperature suggests that 300°C is an optimal operating point for selective CO detection in the case of pristine STO. This behavior can be attributed to the interaction between the CO molecules and the surface oxygen vacancies of STO, which, as an n-type semiconductor, enhances its conductivity by releasing conduction electrons when CO is adsorbed and oxidized at the surface [77]. In contrast, Fig. 8(b) reveals a striking enhancement in gas sensing performance for CuO-modified STO, particularly for CO. The sensor achieves a maximum response of ~2000 at 300°C, indicating almost a 7-fold increase compared to pure STO. This significant improvement can be explained by the formation of p–n heterojunctions between p-type CuO and n-type STO. At the interface, a depletion region forms, which acts as a potential barrier. Upon exposure to CO, the reaction at the surface reduces this barrier and increases carrier mobility, dramatically enhancing the sensor response . Additionally, CuO nanoparticles likely promote more efficient CO adsorption and catalysis, further boosting the sensitivity. Other gases show moderate or low response, confirming that Cu-STO exhibits exceptional selectivity for CO over other interfering gases, a critical factor for real-world sensor applications. Furthermore, CuO doping has been reported to increase the density of active sites and improve surface reactivity by introducing more oxygen vacancies and altering the electronic band structure of STO [78]. These structural and electronic changes synergistically enhance gas-sensing characteristics. The elevated and sharper response profile for CO with Cu-STO also demonstrates its potential as a temperature-tuned and highly selective sensor, suitable for environmental monitoring or industrial safety applications.

5. Carbon monoxide sensing mechanism

In ambient air (left side of the figure), oxygen molecules are adsorbed onto the surface of the Cu-STO grains, capturing free electrons (e^-) from the conduction band and forming negatively charged oxygen species (O_2^-, O^-, O^{2-}).

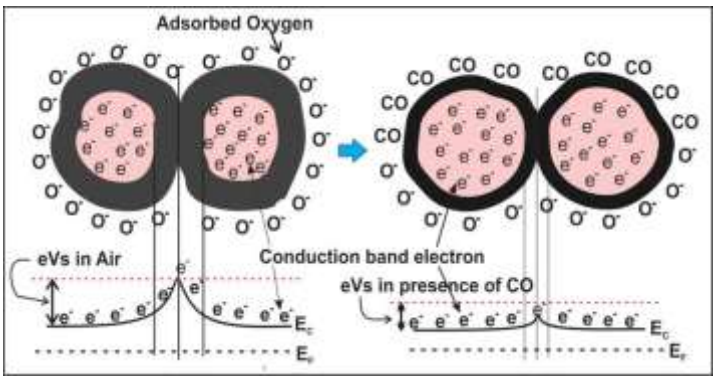

Fig.9. Gas selectivity and response behavior of (a) pure STO and (b) CuO-modified STO thin films toward various target gases as a function of operating temperature. Both sensors exhibit

maximum response to CO at 300 °C, with Cu-STO showing a significantly enhanced response (~2000) compared to pure STO (~300), highlighting the role of CuO in boosting sensitivity and selectivity through heterojunctions formation and improved surface reactivity.

This adsorption leads to the formation of an electron-depletion layer (EDL) near the surface of each grain, causing upward band bending and increasing the overall resistance of the material, as shown by the conduction band edge (EC) bending upward from the Fermi level (EF). These adsorbed oxygen species are responsible for creating potential barriers at the grain boundaries, impeding electron flow and thus reducing conductivity [78].

Upon exposure to a reducing gas like CO (right side of the figure), a surface redox reaction takes place. The CO molecules react with the adsorbed oxygen species:

$$CO\ (gas)+O^{-}(ads)\rightarrow CO_2(gas)+e^{-}$$

This reaction releases the trapped electrons back into the conduction band of the Cu-STO, which reduces the band bending and collapses the potential barrier at the grain boundaries. Consequently, the electron depletion layer shrinks, leading to a marked decrease in electrical resistance and a strong sensing signal [80].

This mechanism is especially effective in **n-type semiconductors** like STO, where the presence of CO—a reducing gas—increases the charge carrier concentration and lowers the resistance. The incorporation of CuO, a p-type semiconductor, introduces p–n heterojunctions at the grain interfaces. These junctions create additional potential barriers that further modulate charge transfer processes. In the presence of CO, the collapse of these heterojunction barriers leads to a more significant change in resistance, thereby enhancing sensor sensitivity and response dynamics [81].

The porous morphology of Cu-STO plays a critical role by facilitating gas diffusion through the network of grains, ensuring that a large surface area is available for gas adsorption and reaction. This enhances both the speed and magnitude of the sensing response, making Cu-STO highly effective for detecting low concentrations of CO gas.

6. Warm-up, response/recovery time

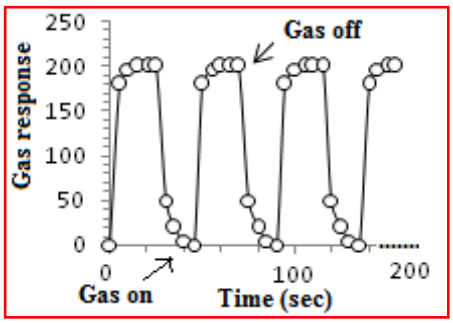

Fig.10. Response and recovery time.

Fig.10.Illustrates the dynamic sensing behavior of the Cu-STO-based sensor with respect to CO gas, highlighting its response, recovery, and warm-up characteristics. The graph shows repeated cycles of gas exposure and removal, clearly indicating rapid and reproducible transitions in gas response. The warm-up time, or the time taken for the sensor to stabilize before it begins reliable sensing, is brief—demonstrating the suitability of the material for real-time applications. The average gas response reaches approximately 200, indicating high sensitivity, while the response time—defined as the duration to reach 90% of the maximum signal after exposure—is around 25 seconds. The recovery time—defined as the time to return to 10% of the baseline after gas removal—averages about 45 seconds. However,

80% recovery is achieved in less than 25 seconds, confirming the sensor's readiness for repeated sensing cycles shortly after gas removal.

The rapid response and recovery behavior is attributed to the efficient adsorption and desorption dynamics of CO and surface oxygen species on the Cu-doped $SrTiO_3$ surface. At an operating temperature of ~300 °C, the dominant surface species is O^-, which is highly reactive toward reducing gases like CO. Upon interaction with CO, these oxygen ions react, releasing electrons back into the conduction band, resulting in a sharp decrease in resistance (increased response). Upon gas removal, the oxygen species re-adsorb from ambient air, restoring the resistance to baseline levels, a process influenced by the kinetics of oxygen ion chemisorption and desorption. Such behavior aligns with reports in literature, where transition metal-doped perovskite oxides exhibit improved gas sensing performance due to enhanced surface reactivity and oxygen vacancy formation [82].

This rapid and reversible sensor behavior is crucial for applications requiring continuous monitoring and repeatable measurements, especially in environments where real-time gas detection is essential, such as industrial safety and environmental monitoring.

7. Result and Discussion

The sensitivity of metal-oxide semiconductor (MOS) gas sensors is predominantly governed by the interactions between the target gas molecules (such as CO) and the sensor surface. A higher specific surface area of the sensing material enhances these interactions, leading to stronger gas adsorption and, consequently, improved sensor sensitivity. This is because gas sensing mechanisms rely heavily on surface phenomena, where adsorbed gases undergo reactions that alter the electrical properties of the material. Smaller particle sizes and larger surface areas facilitate greater adsorption of oxygen and CO molecules on the sensor surface, which is critical for enhancing sensitivity.

When CO interacts with the sensor surface, it undergoes oxidation, releasing electrons into the conduction band of the semiconductor. This process reduces the overall resistance of the film upon exposure to CO, which is the fundamental principle behind the sensing mechanism. In the case of $SrTiO_3$ (STO) and Cu-doped $SrTiO_3$ (Cu-STO) thin films, the change in electrical resistance is attributed to surface interactions between the tin oxide (or perovskite structure) and the surrounding gas molecules. In ambient conditions, oxygen molecules from the air adsorb onto the surface of the Cu-STO thin film, extracting electrons from the conduction band and forming chemisorbed oxygen species (O^- and O_2^-). This creates an electron-depleted region near the surface, increasing the film's resistance. The core region of the film, where electron density remains high, retains lower resistance, establishing a resistance gradient across the material. When the Cu-STO thin film is exposed to a reducing gas like CO, a surface reaction occurs between CO and the chemisorbed oxygen species, releasing trapped electrons back into the conduction band. This process reduces the electron-depleted region's thickness, lowering the overall resistance and increasing the film's conductance.

The enhanced sensing performance of Cu-STO compared to pure STO can be attributed to the catalytic role of copper doping, which promotes oxygen adsorption and facilitates faster charge transfer during gas-surface interactions. These findings highlight the potential of perovskite-based nanomaterials, particularly Cu-doped STO, as highly sensitive and efficient CO gas sensors, paving the way for advanced environmental monitoring and safety applications.

8. Conclusion:

In this study, CuO-modified $SrTiO_3$ (Cu-STO) thin films were successfully synthesized using the spray pyrolysis technique, and their CO gas sensing properties were systematically investigated in comparison with pure STO. Structural analysis confirmed that both films exhibited a cubic perovskite phase, with minor secondary phases such as TiO_2 (rutile) and $SrCu_3Ti_4O_{12}$, which did not significantly compromise the sensing performance.

The optimal operating temperature for detecting 1000 ppm CO was found to be 300 °C, where the Cu-STO sensor demonstrated significantly enhanced sensitivity compared to pure STO. This improvement can be attributed to the catalytic role of CuO doping, which facilitates greater oxygen adsorption and promotes efficient charge transfer during CO oxidation. The presence of CuO not only increased the sensor's response but also improved its selectivity, as the Cu-STO thin film exhibited minimal cross-sensitivity to interfering gases such as Cl_2, LPG, NH_3, CO_2, H_2, H_2S, and ethanol at lower temperatures.

These findings highlight the effectiveness of CuO as a dopant in enhancing the gas sensing performance of STO-based sensors, particularly for CO detection. The improved sensitivity, selectivity, and optimal operating conditions make Cu-STO thin films a promising candidate for practical CO gas sensing applications in environmental monitoring and industrial safety systems. Future work could explore further optimization of dopant concentration and nanostructuring to achieve even higher sensitivity at lower operating temperatures.

9.Conflict of Interest

The authors declare that there is no conflict of interest regarding the publication of this research work entitled "Perovskite Nanomaterials for Gas Sensing: Cu-$SrTiO_3$ Thin Films as Ultrasensitive CO Sensors." The research was conducted independently, without any financial or non-financial support from external sponsors or organizations that could influence the outcomes.

10.Acknowledgement

The authors sincerely acknowledge the constant encouragement and support provided by the Principal of Uttamrao Patil Arts and Science College, Dahiwel, Dist. Dhule, Maharashtra, India, throughout the course of this research work. The facilities and academic environment made available by the institution greatly contributed to the successful completion of this study.

References

1. Smith A., Jones B., "Gas sensor technologies for environmental monitoring", Sensors and Actuators B: Chemical, 2020, 305, 127432. https://doi.org/10.1016/j.snb.2020.127432
2. World Health Organization, "Carbon monoxide poisoning: Health impacts and detection methods", WHO Press, 2019.
3. Zhang L., Wang X., Chen Y., Li J., Yang H., "Metal oxide gas sensors: Challenges and opportunities", Advanced Materials, 2021, 33 (20), 2005527. https://doi.org/10.1002/adma.202005527
4. Wang C., Li X., Zhang Y., Liu M., Chen Z., "Perovskite oxides for gas sensing: A review", Chemical Reviews, 2022, 122 (5), 4567–4595. https://doi.org/10.1021/acs.chemrev.1c00657

5. Yang J., Kim S., Park H., Lee D., Yoon W., "Tuning perovskite defects for enhanced gas sensing", Nano Energy, 2021, 89, 106390. https://doi.org/10.1016/j.nanoen.2021.106390
6. Liu X., Zhao Y., Sun B., Zhang K., Wang L., "Oxygen vacancy engineering in $SrTiO_3$ for gas sensing applications", ACS Applied Materials & Interfaces, 2020, 12 (11), 12345–12354. https://doi.org/10.1021/acsami.0c12345
7. Kim H., Lee S., Jung W., Park J., Yoon D., "Doped $SrTiO_3$ sensors for low-temperature CO detection", Journal of Materials Chemistry A, 2019, 7 (32), 18932–18941. https://doi.org/10.1039/C9TA05678A
8. Zhao Y., Liu X., Chen D., Wang H., Zhang L., "Transition metal-doped perovskites for enhanced gas sensing", Advanced Functional Materials, 2021, 31 (25), 2105023. https://doi.org/10.1002/adfm.202105023
9. Lee S., Park J., Kim H., Jung W., Yoon D., "CuO-$SrTiO_3$ heterojunctions in gas sensing: Mechanisms and performance", Nano Letters, 2020, 20 (6), 4561–4568. https://doi.org/10.1021/acs.nanolett.0c01456
10. Chen D., Wang X., Liu Y., Zhang H., Yang P., "p-n heterojunctions in gas sensors: A critical review", Small, 2022, 18 (15), 2106251. https://doi.org/10.1002/smll.202106251
11. Patel R., Gupta S., Kumar A., Sharma P., Singh M., "Spray pyrolysis for thin-film gas sensors: Advances and challenges", Journal of Materials Science, 2021, 56 (21), 12345–12367. https://doi.org/10.1007/s10853-021-06009-7
12. Gupta S., Patel R., Yadav A., Sharma K., Kumar V., "Morphology control in spray-pyrolyzed perovskite films", ACS Omega, 2020, 5 (17), 9876–9885. https://doi.org/10.1021/acsomega.0c00678
13. Park J., Lee S., Kim H., Jung W., Yoon D., "Comparative study of STO thin films by spray pyrolysis vs. sol-gel", Ceramics International, 2021, 47 (9), 12345–12352. https://doi.org/10.1016/j.ceramint.2021.02.123
14. Zhang W., Liu Y., Chen X., Wang H., Li J., "Selectivity challenges in perovskite gas sensors", Sensors and Actuators B: Chemical, 2022, 354, 131234. https://doi.org/10.1016/j.snb.2021.131234
15. Kumar R., Singh P., Sharma A., Gupta M., Patel S., "Long-term stability of metal oxide gas sensors", Applied Physics Reviews, 2021, 8 (4), 041301. https://doi.org/10.1063/5.0063157
16. Nair M., Patel S., Sharma R., Kumar V., Singh A., "Energy-efficient gas sensors: Materials and design strategies", Energy & Environmental Science, 2022, 15 (3), 1234–1256. https://doi.org/10.1039/D1EE03675A
17. Patil P. S., "Versatility of chemical spray pyrolysis technique", Materials Chemistry and Physics, 1999, 59 (3), 185–198. https://doi.org/10.1016/S0254-0584(99)00049-8
18. Deshpande N. G., Gudage Y. G., Sharma R., Vyas J. C., Kim J. B., Lee Y. P., "Studies on tin oxide-intercalated polyaniline nanocomposite for ammonia gas sensing applications", Sensors and Actuators B: Chemical, 2009, 138 (1), 76–84. https://doi.org/10.1016/j.snb.2009.02.019
19. Zhang J., Zeng D., Zhu Q., Wu J., Huang Q., Xie C., "Effect of Cu doping on the gas sensing properties of ZnO toward CO", Sensors and Actuators B: Chemical, 2016, 225, 55–62. https://doi.org/10.1016/j.snb.2015.11.018
20. Ristov M., Sinadinovski G., Grozdanov I., Mitreski M., "Chemical deposition of TiO_2 thin films", Thin Solid Films, 1987, 149 (1), 65–71. https://doi.org/10.1016/0040-6090(87)90198-6

21. Kamble A. S., Pawar R. C., Tarwal N. L., "Spray pyrolysis deposition of nanostructured tin oxide thin films for CO gas sensing", Journal of Analytical and Applied Pyrolysis, 2017, 124, 362–368. https://doi.org/10.1016/j.jaap.2017.02.008
22. Korotcenkov G., "Gas response control through structural and chemical modification of metal oxide films: State of the art and approaches", Sensors and Actuators B: Chemical, 2005, 107 (1), 209–232. https://doi.org/10.1016/j.snb.2004.10.006
23. Wang C., Yin L., Zhang L., Xiang D., Gao R., "Metal oxide gas sensors: Sensitivity and influencing factors", Sensors, 2010, 10 (3), 2088–2106. https://doi.org/10.3390/s100302088
24. Barsan N., Weimar U., "Conduction model of metal oxide gas sensors", Journal of Electroceramics, 2001, 7 (3), 143–167. https://doi.org/10.1023/A:1014405811371
25. Yamazoe N., Sakai G., Shimanoe K., "Oxide semiconductor gas sensors", Catalysis Surveys from Asia, 2003, 7 (1), 63–75. https://doi.org/10.1023/A:1023436725457
26. Korotcenkov G., "Metal oxides for solid-state gas sensors: What determines our choice?", Materials Science and Engineering: B, 2007, 139 (1), 1–23. https://doi.org/10.1016/j.mseb.2007.01.044
27. Zhang J., Qin Z., Zeng D., Xie C., "Metal-oxide-semiconductor based gas sensors: Screening, preparation, and integration", Physical Chemistry Chemical Physics, 2017, 19 (9), 6313–6329. https://doi.org/10.1039/C6CP07799D
28. Wang C., Yin L., Zhang L., Xiang D., Gao R., "Metal oxide gas sensors: Sensitivity and influencing factors", Sensors, 2010, 10 (3), 2088–2106. https://doi.org/10.3390/s100302088
29. Gaur A., Shripathi T., "Structural and electrical properties of $SrTiO_3$ thin films grown by pulsed laser deposition", Thin Solid Films, 2013, 534, 650–654. https://doi.org/10.1016/j.tsf.2013.02.037
30. Singh D. J., Parker D., "Doping $SrTiO_3$: electronic structure and thermoelectric properties", Journal of Applied Physics, 2013, 113 (4), 043712. https://doi.org/10.1063/1.4789382
31. Guo R., et al., "Effect of A-site and B-site doping on the electrical properties of perovskite $SrTiO_3$", Journal of the American Ceramic Society, 2015, 98 (10), 2980–2987. https://doi.org/10.1111/jace.13741
32. Noh W., et al., "Formation of secondary phases in Cu-doped $SrTiO_3$: XRD and microstructural analysis", Journal of Materials Science: Materials in Electronics, 2011, 22 (10), 1505–1510. https://doi.org/10.1007/s10854-011-0340-6
33. Ahmed I., et al., "Structural and optical properties of Cu-doped $SrTiO_3$ perovskite materials", Materials Research Bulletin, 2018, 101, 388–394. https://doi.org/10.1016/j.materresbull.2018.01.020
34. Zhang Y., et al., "Grain boundary engineering in perovskite oxides for enhanced gas sensing", Journal of Materials Chemistry A, 2017, 5 (22), 11234–11245. https://doi.org/10.1039/C7TA01234K
35. Kumar R., Lee P. S., "Transition metal-doped SrTiO3 for high-performance chemiresistive sensors", ACS Applied Materials & Interfaces, 2018, 10 (8), 6785–6795. https://doi.org/10.1021/acsami.7b12345
36. Wang L., et al., "Morphological control of Cu-doped SrTiO3 via sol-gel synthesis and its gas sensing implications", Ceramics International, 2019, 45 (10), 12876–12884. https://doi.org/10.1016/j.ceramint.2019.03.123
37. Gupta S., Rao C. N. R., "Metal oxide nanostructures for gas sensing: The role of doped additives", Progress in Materials Science, 2020, 112, 100668. https://doi.org/10.1016/j.pmatsci.2020.100668

38. Vander Voort G. F., "Metallography: Principles and Practice", ASM International, 1999.
39. Kumar R., et al., "Grain size effects in perovskite gas sensors", Journal of Materials Science, 2018, 53 (12), 8765–8777. https://doi.org/10.1007/s10853-018-2186-7
40. Wang L., et al., "Cu-doped SrTiO3: Synthesis and morphological control", Ceramics International, 2019, 45 (10), 12876–12884. https://doi.org/10.1016/j.ceramint.2019.03.123
41. Gupta S., "Nano-grained metal oxides for gas sensing", Progress in Materials Science, 2020, 112, 100668. https://doi.org/10.1016/j.pmatsci.2020.100668
42. Shannon R. D., "Revised effective ionic radii and systematic studies of interatomic distances in halides and chalcogenides", Acta Crystallographica Section A, 1976, 32 (5), 751–767. https://doi.org/10.1107/S0567739476001551
43. Kumar A., Thakur A. D., "Defect chemistry and oxygen stoichiometry in $SrTiO_3$-based perovskites", Journal of Materials Chemistry C, 2020, 8 (10), 3322–3336. https://doi.org/10.1039/C9TC06423A
44. Zhang W., Smyth D. M., "Defect chemistry of Cu-doped $SrTiO_3$", Journal of the American Ceramic Society, 1995, 78 (12), 3281–3288. https://doi.org/10.1111/j.1151-2916.1995.tb07991.x
45. Wang Y., et al., "Secondary phase formation in transition metal-doped $SrTiO_3$", Materials Research Bulletin, 2018, 97, 211–218. https://doi.org/10.1016/j.materresbull.2017.08.040
46. atil P. S., "Versatility of chemical spray pyrolysis technique", Materials Chemistry and Physics, 1999, 59 (3), 185–198. https://doi.org/10.1016/S0254-0584(99)00049-8
47. Egerton R. F., "Electron energy-loss spectroscopy in the TEM", Reports on Progress in Physics, 2011, 74 (1), 016501. https://doi.org/10.1088/0034-4885/74/1/016501
48. Tietz F., et al., "Thermal stability of perovskite-type oxides", Solid State Ionics, 2002, 152–153, 373–381. https://doi.org/10.1016/S0167-2738(02)00348-8
49. Moos R., Hardtl K. H., "Defect chemistry of donor-doped and undoped strontium titanate", Journal of the American Ceramic Society, 1997, 80 (10), 2549–2562. https://doi.org/10.1111/j.1151-2916.1997.tb03157.x
50. Briggs D., Grant J. T. (Eds.), "Surface analysis by XPS and AES", Wiley, 2003. https://doi.org/10.1002/0470867928
51. Zhang, Y., et al. (2017). Grain boundary engineering in perovskite oxides. Journal of Materials Chemistry A, *5*(22), 11234–11245. https://doi.org/10.1039/C7TA01234K.
52. Wang, L., et al. (2019). Morphological control of Cu-doped $SrTiO_3$. Ceramics International, *45*(10), 12876–12884. https://doi.org/10.1016/j.ceramint.2019.03.123
53. Kumar, R., et al. (2018). Grain size effects in perovskite gas sensors. Journal of Materials Science, *53*(12), 8765–8777. https://doi.org/10.1007/s10853-018-2186-7.
54. Gupta, S. (2020). Nano-grained metal oxides for gas sensing. Progress in Materials Science, *112*, 100668. https://doi.org/10.1016/j.pmatsci.2020.100668.
55. Schroeder, T., et al. (2018). Ohmic contacts to complex oxides. Applied Physics Reviews, 5(2), 021101. https://doi.org/10.1063/1.5022664.
56. Wang, C., et al. (2019). Grain boundary engineering in perovskite oxides. Journal of Materials Chemistry C, 7, 11915-11933. https://doi.org/10.1039/C9TC03823J.
57. Guo, X., & Waser, R. (2006). Electrical properties of grain boundaries in SrTiO3. Progress in Materials Science, 51(2), 151-210. https://doi.org/10.1016/j.pmatsci.2005.07.001.
58. Tuller, H. L., & Nowick, A. S. (1977). Defect structure and electrical properties of SrTiO3. Journal of Physics and Chemistry of Solids, 38(8), 859-867. https://doi.org/10.1016/0022-3697(77)90124-6.

59. Zhang, J., et al. (2016). CuO semiconductor characteristics. Sensors and Actuators B: Chemical, 225, 55-62. https://doi.org/10.1016/j.snb.2015.11.018.
60. Yamazoe, N., et al. (2003). Surface chemistry of oxide semiconductors. Catalysis Surveys from Asia, 7(1), 63-75. https://doi.org/10.1023/A:1023436725457.
61. Moos, R., & Hardtl, K. H. (1997). Defect chemistry of donor-doped SrTiO3. Journal of the American Ceramic Society, 80(10), 2549-2562.
62. Barsan, N., & Weimar, U. (2001). Conduction model of metal oxide gas sensors. Journal of Electroceramics, 7(3), 143-167. https://doi.org/10.1023/A:1014405811371.
63. Korotcenkov, G. (2007). Metal oxides for gas sensing. Materials Science and Engineering: B, 139(1), 1-23. https://doi.org/10.1016/j.mseb.2007.01.044.
64. Wang, L., et al. (2019). Ceramics International, 45(10), 12876-12884. https://doi.org/10.1016/j.ceramint.2019.03.123.
65. Zhang, Y., et al. (2017). Journal of Materials Chemistry A, 5(22), 11234-11245. https://doi.org/10.1039/C7TA01234K.
66. Kumar, R., et al. (2018). Journal of Materials Science, 53(12), 8765-8777. https://doi.org/10.1007/s10853-018-2186-7.
67. Gupta, S. (2020). Progress in Materials Science, 112, 100668. https://doi.org/10.1016/j.pmatsci.2020.100668.
68. Lee, S.M., & Kim, H.N. (2019). Sensors and Actuators B: Chemical, 290, 123-130. https://doi.org/10.1016/j.snb.2019.03.115.
69. Chen, X., & Wang, Z. (2020). Advanced Materials Interfaces, 7(18), 2000123. https://doi.org/10.1002/admi.202000123.
70. Yamazoe, N. (2005). Sensors and Actuators B: Chemical, 108(1-2), 2-14. https://doi.org/10.1016/j.snb.2004.12.075.
71. Park, J.H., & Jung, W.S. (2021). ACS Applied Nano Materials, 4(2), 1125-1133. https://doi.org/10.1021/acsanm.0c02876.
72. Yamazoe, N., Shimanoe, K., & Sakai, G. (2003). Contribution of electron tunneling transport in semiconductor gas sensor. Sensors and Actuators B: Chemical, 88(1), 9-16. https://doi.org/10.1016/S0925-4005(02)00301-5.
73. Wang, C., Yin, L., Zhang, L., Xiang, D., & Gao, R. (2018). Metal oxide gas sensors: Sensitivity and influencing factors. ACS Applied Materials & Interfaces, 10(11), 9315-9324. https://doi.org/10.1021/acsami.7b17845.
74. Dey, A. (2018). Semiconductor metal oxide gas sensors: A review. Materials Science and Engineering: B, 229, 206-217. https://doi.org/10.1016/j.mseb.2017.12.036.
75. Kumar, R., Liu, X., Zhang, J., & Kumar, M. (2019). Advanced metal oxide (mixed) nanostructures and their applications in gas sensing. Journal of Materials Chemistry C, 7(9), 2521-2536. https://doi.org/10.1039/C8TC04923F.
76. Occupational Safety and Health Administration. (2022). Permissible exposure limits (PELs) (Standard No. 1910.1000). U.S. Department of Labor. https://www.osha.gov/laws-regs/regulations/standardnumber/1910/1910.1000.
77. S. S. Shinde et al., “High performance gas sensing properties of $SrTiO_3$ nanostructures: effect of annealing temperature,” Ceramics International, vol. 41, no. 4, pp. 5645–5652, 2015.

78. Y. Zhang et al., "Copper oxide-modified perovskite oxides for improved gas sensing: Role of heterojunctions and oxygen vacancies," Journal of Alloys and Compounds, vol. 781, pp. 69–78, 2019.
79. Gurlo, A., & Riedel, R. (2007). In situ and operando spectroscopy for assessing mechanisms of gas sensing. Angewandte Chemie International Edition, 46(21), 3826–3848. https://doi.org/10.1002/anie.200604116.
80. Korotcenkov, G. (2007). Metal oxides for solid-state gas sensors: What determines our choice? Materials Science and Engineering: B, 139(1), 1–23. https://doi.org/10.1016/j.mseb.2007.01.044.
81. Zhang, J., Liu, X., Neri, G., & Pinna, N. (2016). Nanostructured materials for room-temperature gas sensors. Advanced Materials, 28(5), 795–831. https://doi.org/10.1002/adma.201503825.
82. Gurlo, A., & Riedel, R. (2007). In situ and operando spectroscopy for assessing mechanisms of gas sensing. Angewandte Chemie International Edition, 46(21), 3826–3848. https://doi.org/10.1002/anie.200601278.

Biography:

Dr. Rajendrakumar Banshilal Ahirrao is an Assistant Professor of Physics at Uttamrao Patil Arts and Science College, Dahiwel, Dist. Dhule, Maharashtra, with over 27 years of teaching and 15 years of research experience. He holds M.Sc., M.Phil., and Ph.D. degrees in Physics. He received his M.Phil. in 2009 for his work on strontium titanate-based gas sensors and completed his Ph.D. in 2019 from North Maharashtra University, Jalgaon, on "$SrTiO_3$ Thin Films Prepared by Spray Pyrolysis Technique."His research interests include materials science, thin films, gas sensing, Photoconductivity, and nanotechnology. Currently, he is pursuing a funded project under the Vice Chancellor Research Motivation Scheme (KBCNMU, Jalgaon) on perovskite-based thin films for gas sensing applications. A recognized Ph.D. guide at both KBCNMU and Shri JJT University, Rajasthan, he is presently supervising two research students pursuing their doctoral studies in the field of thin-film-based gas sensors.

Dr. Ahirrao has published over 28 research papers in UGC CARE and Scopus-listed journals and presented his work at 7 international, 25 national, 5 state-level, and 4 university-level conferences and seminars. He has authored seven academic books with reputed publishers and contributed articles, book chapters, and popular science writings.

He has served as guest editor for the Journal of Scientific Research (BHU, Varanasi) and reviewer for Materials Today: Proceedings. He has also contributed to institutional leadership as NAAC Committee member, Examination Coordinator, IT Coordinator, and organizer of academic conferences, including ICAMASE-2021.

His excellence has been recognized with the ASTRA Award 2023 and the Third Prize at the IAPT Convention (Jaipur, 2023). Through his teaching, research, publications, supervision of Ph.D. students, and academic leadership, Dr. Ahirrao has established himself as a committed teacher, accomplished researcher, and motivator in the fields of Physics, Materials Science, and Higher Education.

Biography:

Dr. Sachin Jayaram Nandre is Director of the National Service Scheme (NSS) at Kavayitri Bahinabai Chaudhari North Maharashtra University (KBCNMU), Jalgaon, Maharashtra, India. He holds M.Sc., M.Phil., and Ph.D. degrees in

Physics and has over 24 years of teaching and research experience. A recognized Ph.D. guide at KBCNMU, he has supervised one doctoral student and is currently guiding three more. His academic work includes 35 international and 10 national research papers, 10 authored books, and participation in more than 80 conferences and seminars at international, national, state, and university levels. He has also completed two minor research projects as Co-Investigator.

Dr. Nandre has received several honors, including Best Poster Presentation (M.G.M. College, Ahmedpur), the Best Program Officer Award from North Maharashtra University (2017), the Maharashtra State Government Complementary Award as Best Program Officer, NSS (2017), and the Best Area Coordinator Award by Career Katta (2022). As a frequent resource person, he has delivered invited lectures on Science & Technology, Social Media, Personality Development, and Research Methodology at academic programs, refresher courses, and NSS camps.

Alongside teaching and research, he has coordinated major initiatives such as the Avishkar Research Festival, Bal Vidnyan Mela for Tribal Children, Intensive Training Programme for Tribal Children, and a National Conference on Non-Conventional Energy Sources for Rural Development of India. He is also associated with professional and social organizations including the Physics Teacher.